NASA Contractor Report 198514

Active Control of Fan Noise: Feasibility Study

Volume 6: Theoretical Analysis for Coupling of Active Noise Control Actuator Ring Sources to an Annular Duct with Flow

R.E. Kraft
General Electric Aircraft Engines
Cincinnati, Ohio

September 1996

Prepared for
Lewis Research Center
Under Contract NAS3–26617

National Aeronautics and
Space Administration

Active Control of Fan Noise: Feasibility Study
Volume 6: Theoretical Analysis for Coupling of Active Noise Control Actuator Ring Sources to an Annular Duct with Flow

Summary

The objective of this effort is to develop an analytical model for the coupling of active noise control (ANC) piston-type actuators that are mounted flush to the inner and outer walls of an annular duct to the modes in the duct generated by the actuator motion. The analysis will be used to couple the ANC actuators to the modal analysis propagation computer program for the annular duct, to predict the effects of active suppression of fan-generated engine noise sources. This combined program will then be available to assist in the design or evaluation of ANC systems in fan engine annular exhaust ducts.

An analysis has been developed to predict the modes generated in an annular duct due to the coupling of flush-mounted ring actuators on the inner and outer walls of the duct. The analysis has been combined with a previous analysis for the coupling of modes to a cylindrical duct in a FORTRAN computer program to perform the computations. The method includes the effects of uniform mean flow in the duct. The program can be used for design or evaluation purposes for active noise control hardware for turbofan engines.

Predictions for some sample cases modeled after the geometry of the NASA Lewis ANC Fan indicate very efficient coupling in both the inlet and exhaust ducts for the $m = 6$ spinning mode at frequencies where only a single radial mode is cut-on. Radial mode content in higher order cut-off modes at the source plane and the required actuator displacement amplitude to achieve 110 dB SPL levels in the desired mode were predicted. Equivalent cases with and without flow were examined for the cylindrical and annular geometry, and little difference was found for a duct flow Mach number of 0.1.

The actuator ring coupling program will be adapted as a subroutine to the cylindrical duct modal analysis and the exhaust duct modal analysis. This will allow the fan source to be defined in terms of characteristic modes at the fan source plane and predict the propagation to the arbitrarily-located ANC source plane. The actuator velocities can then be determined to generate the anti-phase mode. The resulting combined fan source/ANC pressure can then be calculated at any desired wall sensor position. The actuator velocities can be determined manually or using a simulation of a control system feedback loop. This will provide a very useful ANC system design and evaluation tool.

Active Control of Fan Noise: Feasibility Study
Volume 6: Theoretical Analysis for Coupling of Active Noise Control Actuator Ring Sources to an Annular Duct with Flow

Table of Contents

1. Introduction 1
   1.1 Program Objective 1
   1.2 Previous Effort 1
   1.3 Duct Geometry 1
   1.4 Assumptions 2
   1.5 Approach 3
   1.6 Summary of Results 3
2. Analysis of ANC Actuator Coupling to an Annular Duct 4
   2.1 Wave Equation for the Acoustic Pressure 4
   2.2 Boundary Condition with Slip Flow 5
   2.3 Transformation to a Non-Homogeneous Differential Equation with Homogeneous Boundary Conditions 8
   2.4 Derivation of the Non-Homogeneous Differential Equation in z 11
   2.5 Fourier Transform for z-Dependence 15
   2.6 Solution for the Acoustic Pressure Field Generated by the Actuators 19
3. Solution for Box Function Actuator 20
   3.1 Choice of Box Function Actuator Velocity Profile 20
   3.2 Sample Computations for Box Function Case 21
      3.2.1 Computer Output for Case 1, Cylindrical Duct, Mach 0.0, m = 6 22
      3.2.2 Computer Output for Case 2, Annular Duct, Mach 0.0, m = 6, Outer Wall Actuator Only 25
      3.2.3 Comparison of Cases 1 and 3 27
      3.2.4 Comparison of Cases 2 and 4 27
      3.2.5 Comparison of Cases 4 and 5 28
      3.2.6 Comparison of Cases 4 and 6 29
      3.2.7 Comparison of Cases 7 and 8 30
      3.2.8 Discussion of Case 9 31
4. Conclusions and Recommendations 34
   4.1 Conclusions 34
   4.2 Recommendations for Further Effort 34
5. Appendices 36
   5.1 Appendix A - Numerical Computation of Bessel Function Integrals 36
   5.2 Appendix B - Contour Integrations for Inversion of Fourier Integrals 37
6. References 40

Active Control of Fan Noise: Feasibility Study
Volume 6: Theoretical Analysis for Coupling of Active Noise Control Actuator Ring Sources to an Annular Duct with Flow

1. Introduction

1.1 Program Objective

The objective of this effort is to develop an analytical model for the coupling of active noise control (ANC) piston-type actuators that are mounted flush to the inner and outer walls of an annular duct to the modes in the duct generated by the actuator motion. The analysis will be used to couple the ANC actuators to the modal analysis propagation computer program for the annular duct, to predict the effects of active suppression of fan-generated engine noise sources. This combined program will then be available to assist in the design or evaluation of ANC systems in fan engine annular exhaust ducts.

1.2 Previous Effort

In a prior analysis[1], a model was developed for the coupling of ANC sources to a cylindrical duct, more representative of a turbofan inlet. The reader is referred to that paper for background on prior research and motivation for the application of ANC systems to aircraft engines.

The previous analysis did not account for the effects of mean flow, which is included in this analysis. The present study is based in large part on the development presented in the previous paper, extending the analysis to include annular duct geometry with ANC actuators on both inner and outer walls and the effects of uniform mean flow. The results apply to both cylindrical and annular ducts, with or without mean flow. The extension to annular ducts provides a first approximation to simulating a fan exhaust system.

1.3 Duct Geometry

Figure (1). shows the duct geometry and the mounting positions for the actuator rings. The radial variable is r, the angular variable is θ, and the axial variable is z. The duct inner and outer radii are given by r_1 and r_2, respectively. The actuator ring has axial extent L, and the zero of the axial coordinate system is taken as the upstream end of the actuator ring. The mean flow velocity is denoted as U, and the flow is positive when moving in the direction of the positive z-axis (exhaust duct flow will be positive, inlet duct flow will be negative).

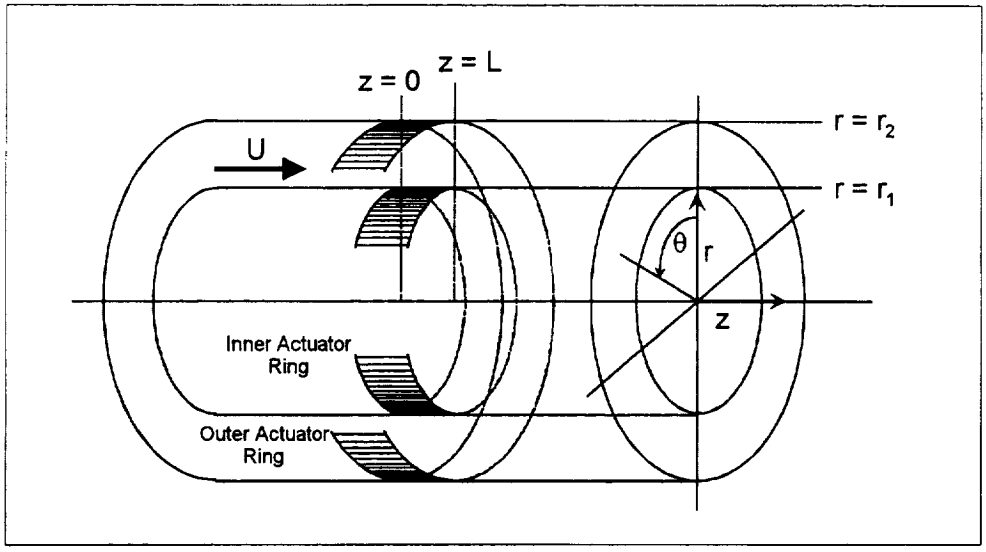

Figure (1). Annular geometry for ANC actuator mounting.

1.4 Assumptions

The analysis is subject to a number of idealizations and simplifying assumptions. Among these are:

1. The duct geometry is axisymmetric and is assumed to be constant in inner and outer radii along the full length of the duct.
2. The mean flow is assumed to have a uniform profile, that is, contains no shear layers.
3. The actuators are rectangular in shape, and behave like rigid pistons, achieving a volume velocity equivalent to a piston mounted flush to the wall.
4. It is assumed that there is no interaction between the propagating fan-source-generated mode passing the actuator rings and the pistons, that is, the pistons are assumed to have infinite internal impedance.

The program is meant primarily for computing the case in which only one radial mode is cut-on. The actuator velocity that generates the first radial mode that matches the fan source mode is found. The complex ratio of inner actuator velocity to outer actuator velocity is given, and this ratio is maintained throughout the computation as the outer wall actuator velocity is scaled. The program solution determines the pressure (modal) spillover into higher-order cut-off modes at the actuator source plane. Although these modes do not propagate, the smaller their value the more efficient is the coupling of the actuators to the desired mode.

The program can also be used for the case with multiple cut-on radial modes, but the computation attempts to match only the first radial mode to the input SPL level. The given inner actuator velocity to outer actuator velocity ratio is maintained throughout the computation. The mode coefficient obtained for the second radial mode will depend on the velocity chosen for the inner actuator, but the program does not attempt to find the

inner actuator velocity that best matches both fan source mode coefficients simultaneously. This, in fact, may be a very difficult problem to solve.

1.5 Approach

The approach will be to use a classical modal solution to the wave equation in an annular duct with non-homogeneous boundary conditions. A transformation of variables method is applied that transforms the homogeneous differential equation with non-homogeneous boundary conditions to a non-homogeneous differential equation with homogeneous boundary conditions, which is more tractable. A modal expansion in hardwall duct modes is used to solve the radial variation and the axial variation is solved using infinite Fourier Transforms. This is similar to the approach in Reference 1, with the extension to more complex annular geometry and the inclusion of the effects of mean flow.

1.6 Summary of Results

An analysis has been developed that predicts the modes generated in an annular duct due to the coupling of flush-mounted ring actuators on the inner and outer walls of the duct. The analysis has been combined with a previous analysis for the coupling of modes to a cylindrical duct in a FORTRAN computer program which is operational and partially validated. The method includes the effects of uniform mean flow in the duct. The program can be used for design or evaluation purposes for active noise control hardware for turbofan engines.

Predictions for some sample cases modeled using the geometry of the NASA Lewis ANC Fan indicate very efficient coupling in both the inlet and exhaust ducts for the $m = 6$ spinning mode at frequencies where only a single radial mode is cut-on. Radial mode content in higher order cut-off modes at the source plane and the required actuator displacement amplitude to achieve 110 dB SPL levels in the desired mode were predicted. Equivalent cases with and without flow were examined for the cylindrical and annular geometry, and little difference was found for a duct flow Mach number of 0.1. The use of the inner ring of actuators to improve coupling efficiency to a single radial mode and to couple to two radial modes simultaneously was examined.

2. Analysis of ANC Actuator Coupling to an Annular Duct

2.1 Wave Equation for the Acoustic Pressure

The partial differential equation for the acoustic pressure in a duct with uniform mean flow is given by

$$\left(\frac{\partial}{\partial t}+U\frac{\partial}{\partial z}\right)^2 p = c^2\nabla^2 p \tag{1}$$

where

t	=	time
z	=	axial variable
p	=	acoustic pressure
c	=	speed of sound
U	=	mean flow velocity in the z- direction

Using the Laplacian operator in a cylindrical coordinate system and postulating harmonic time dependence of the form

$$p(t) = e^{-i\omega t} \tag{2}$$

where

i	=	$\sqrt{-1}$
ω	=	circular frequency, = $2\pi f$
f	=	frequency, Hz.,

we can write Equation (1) in the form

$$\frac{1}{c^2}\left(-i\omega+U\frac{\partial}{\partial z}\right)^2 p = \frac{1}{r}\frac{\partial}{\partial r}\left(r\frac{\partial}{\partial r}\right)+\frac{1}{r^2}\frac{\partial^2 p}{\partial\theta^2}+\frac{\partial^2 p}{\partial z^2} \tag{3}$$

where

r	=	radial variable
θ	=	circumferential variable.

The periodic boundary condition in θ allows us to separate the θ-dependence of the solution in the form

$$p(r, z, \theta) = p(r, z)e^{im\theta} \tag{4}$$

where

m = spinning mode order, any positive or negative integer or zero

When Equation (4) is substituted into the partial differential equation, this further reduces the form to

$$\frac{1}{r}\frac{\partial}{\partial r}\left(r\frac{\partial p}{\partial r}\right) - \frac{m^2}{r^2}p + 2ikM\frac{\partial p}{\partial z} + \left(1 + M^2\right)\frac{\partial^2 p}{\partial z^2} + k^2 p = 0 \tag{5}$$

where

k = wavenumber, = ω/c (constant)
M = mean flow Mach number, = U/c (constant)

This is the homogeneous partial differential equation in the radial and axial variables. The solution for p in r and z must satisfy this equation and the boundary conditions applied by the actuators at their locations on the inner and outer walls of the duct.

2.2 Boundary Condition with Slip Flow

The actuators will be modeled as rigid pistons of rectangular shape that vibrate with infinite internal impedance at frequency ω. On the actuator surface, the wall has a radial velocity component denoted by v_w. The boundary condition, which must include the effects of slip flow at the wall surface, will be written in terms of the requirement that the normal component of acoustic particle displacement be continuous at the wall (it should be noted that the physically incorrect assumption of slip flow leads to the anomaly of different boundary conditions depending on whether particle displacement or particle velocity continuity is assumed[2]).

The normal velocity of the actuator surface at the wall is related to the surface displacement for harmonic time dependence as

$$v_w = -i\omega\zeta \tag{6}$$

where ζ denotes either the actuator surface displacement or the acoustic particle displacement at the wall. The acoustic particle velocity at the wall is written in terms of the acoustic particle displacement using the convected derivative,

$$v_r = \left(-i\omega + U\frac{\partial}{\partial z}\right)\zeta \tag{7}$$

where v_r is the radial component of the acoustic velocity.

The radial component of the acoustic momentum equation is given by

$$\frac{\partial p}{\partial r} = i\rho\omega v_r - \rho U\frac{\partial v_r}{\partial z} \tag{8}$$

where ρ is the ambient air density. The assumption of continuity of particle displacement at the wall requires that the actuator displacement be the same as the normal component of acoustic particle displacement. Combining Equations (6) and (7) gives the relation between actuator normal velocity and the acoustic particle velocity normal to the wall.

$$v_r = \left(1 + i\frac{M}{k}\frac{\partial}{\partial z}\right)v_w \tag{9}$$

Substituting the expression for the acoustic velocity at the wall into the momentum equation gives the boundary condition for the pressure at the wall

$$\frac{\partial p}{\partial r} = i\frac{\rho c}{k}\left[k + iM\frac{\partial}{\partial z}\right]^2 v_w \tag{10}$$

The actuator velocity at the wall can be Fourier-analyzed into its various spinning mode components in the circumferential direction, which will depend on the functional form of the actuator velocity in θ

$$v_w(\theta) = \sum_{m=-\infty}^{\infty} v_{wm} e^{im\theta} \tag{11}$$

where v_{wm} is the m-order component of the actuator circumferential velocity profile at the wall. This expansion and a method to determine the v_{wm} to generate a preferred m-order were the considered in Kraft and Kontos[3]. For this analysis, we assume that only a single m-order is under consideration, and that the m-order component of the actuator wall velocity variation has been determined and is given.

The actuator velocity at the inner and outer walls can be expressed in terms of the m-order spinning mode component and the axial velocity profile as

$$v_{lw} = v_{lm} h(z) \tag{12}$$

and

$$v_{2w} = v_{2m} h(z) \tag{13}$$

where subscript 1 refers to the inner wall, subscript 2 refers to the outer wall, and h(z) is the dimensionless axial functional dependence of the actuator velocity.

The boundary condition equation at the inner wall can then be written

$$\left.\frac{\partial p}{\partial r}\right|_1 = -\left(1 + \frac{iM}{k}\frac{\partial}{\partial z}\right)^2 A_{1m} h(z) \qquad \text{at } r = r_1, \quad 0 \le z \le L \tag{14}$$

and the boundary condition at the outer wall can be written

$$\left.\frac{\partial p}{\partial r}\right|_2 = \left(1 + \frac{iM}{k}\frac{\partial}{\partial z}\right)^2 A_{2m} h(z) \qquad \text{at } r = r_2, \quad 0 \le z \le L \tag{15}$$

where we define the m^{th} order coefficient of the wall velocity at the inner wall as

$$A_{1m} = -i\rho c k v_{1m} \tag{16}$$

and the m^{th} order coefficient of the wall velocity at the outer wall as

$$A_{2m} = -i\rho c k v_{2m} \tag{17}$$

We have made an implicit assumption here that leading and trailing edges of the inner and outer rings align at the same axial stations. Later it will be shown that this is necessary to simplify the analysis. Rings that do not align axially can be considered separately and the generated pressure fields will add linearly.

We shall also refer to the effective volume velocity of the actuator rings, which is defined at the inner wall as

$$V_{1m} = e^{im\theta} \int_0^L v_{1m} h(z) dz \tag{18}$$

and at the outer wall as

$$V_{2m} = e^{im\theta} \int_0^L v_{2m} h(z) dz \tag{19}$$

For the purposes of this analysis, we assume that the duct walls adjoining the actuator rings at both the inner and outer walls are hard, so that the boundary condition away from the actuator region is given by

$$\frac{\partial p}{\partial r} = 0 \qquad \text{at} \quad r = r_1 \quad \text{and} \quad r = r_2 \quad \text{for} \quad z < 0 \quad \text{and} \quad z > L \tag{20}$$

2.3 Transformation to a Non-Homogeneous Differential Equation with Homogeneous Boundary Conditions

The objective is to transform the homogeneous differential equation with non-homogeneous boundary conditions into a non-homogeneous differential equation with homogeneous boundary conditions. This is accomplished using a three-dimensional transformation of variables for the acoustic pressure of the form

$$f(r,\theta,z) = p(r,\theta,z) - g(r,\theta,z) \tag{21}$$

where $g(r,\theta,z)$ is chosen to be an otherwise arbitrary function that satisfies the non-homogeneous boundary conditions.

The choice we shall make for $g(r,\theta,z)$ is a quadratic form in r:

$$g(r,\theta,z) = \left[B_1 r + B_2 r^2\right] e^{im\theta} h(z) \tag{22}$$

where B_1 and B_2 are undetermined constants. Then, at $r = r_1$,

$$\frac{\partial g}{\partial r} = \left[B_1 + 2B_2 r_1\right] e^{im\theta} h(z) \tag{23}$$

and at $r = r_2$,

$$\frac{\partial g}{\partial r} = \left[B_1 + 2B_2 r_2\right] e^{im\theta} h(z) \tag{24}$$

We want to show that $f(r,\theta,z)$ satisfies homogeneous boundary conditions at r_1 and r_2. The radial derivative of f at $r = r_1$ can be written as

$$\frac{\partial f}{\partial r} = \frac{\partial p}{\partial r} - \frac{\partial g}{\partial r} = \left(1 + i\frac{M}{k}\frac{\partial}{\partial z}\right)^2 A_{2m} h(z) - \left[B_1 + 2B_2 r_1\right] h(z) \tag{25}$$

where Equation (15) for the boundary condition in p and Equation (24) for the boundary condition in g have been substituted and the common $e^{im\theta}$ factor has been divided out. Similarly, the radial derivative of f at $r = r_2$ can be written as

$$\frac{\partial f}{\partial r} = \frac{\partial p}{\partial r} - \frac{\partial g}{\partial r} = \left(1 + i\frac{M}{k}\frac{\partial}{\partial z}\right)^2 A_{2m}h(z) - \left[B_1 + 2B_2 r_2\right]h(z) \tag{26}$$

To get homogeneous boundary conditions in f, we set

$$\frac{\partial f}{\partial r} = 0 \qquad \text{at} \quad r = r_1 \quad \text{and} \quad r = r_2 \tag{27}$$

Carrying out the derivatives of h(z) from the square of the convected derivative in Equations (25) and (26), we can define a function

$$H_M(z) = 1 + 2i\frac{M}{k}\frac{h'}{h} - \left(\frac{M}{k}\right)^2 \frac{h''}{h} \tag{28}$$

where the primes denote differentiation with respect to z. Equations (25) and (26), then, are two equations in two unknowns for B_1 and B_2, which can be solved to give

$$B_1 = H_M A_{2m} - \frac{H_M(A_{2m} - A_{1m})}{r_2 - r_1} r_2 \tag{29}$$

and

$$B_2 = \frac{H_M(A_{2m} - A_{1m})}{2(r_2 - r_1)} \tag{30}$$

Note that B_1 and B_2 are functions of z. With the coefficients B_1 and B_2, the function g is completely determined, and the function f satisfies homogeneous (zero derivative) boundary conditions.

It remains to derive the differential equation that f must satisfy. This is found by substituting Equation (21) for p into the differential equation. After a fair amount of algebra, the result can be shown to be

$$\frac{1}{r}\frac{\partial}{\partial r}\left(r\frac{\partial f}{\partial r}\right)-\frac{m^2}{r^2}f+2ikM\frac{\partial f}{\partial z}+\left(1+M^2\right)\frac{\partial^2 f}{\partial z^2}+k^2 f=$$

$$\left[\left(\frac{m^2-1}{r}-k^2 r\right)B_1+\left(4+m^2-k^2r^2\right)B_2\right]h-2ikMr\left[B_1+rB_2\right]h'-\left(1-M^2\right)r\left[B_1+rB_2\right]h'' \tag{31}$$

This is the non-homogeneous partial differential equation that must be satisfied by the function f, which, by virtue of the particular choice of g, has homogeneous boundary conditions.

For convenience, we shall write the differential operator on the left-hand-side of Equation (31) as

$$\mathcal{L}(\,)=\frac{1}{r}\frac{\partial}{\partial r}\left(r\frac{\partial}{\partial r}\right)-\frac{m^2}{r^2}+2ikM\frac{\partial}{\partial z}+\left(1+M^2\right)\frac{\partial^2}{\partial z^2}+k^2 \tag{32}$$

The right-hand-side of the differential equation can also be written in a somewhat easier to grasp form as

$$Q(r,z)=D_1\frac{1}{r}+D_2+D_3 r+D_4 r^2 \tag{33}$$

where

$$D_1(z)\equiv\left(m^2-1\right)B_1 h \tag{34}$$

$$D_2(z)\equiv\left(4+m^2\right)B_2 h \tag{35}$$

$$D_3(z)\equiv-\left[k^2 h+2ikMh'+\left(1-M^2\right)h''\right]B_1 \tag{36}$$

and

$$D_4(z)\equiv-\left[k^2 h+2ikMh'+\left(1-M^2\right)h''\right]B_2 \tag{37}$$

Using Equations (32) and (33), the differential equation can now be written simply as

$$\mathcal{L}(f)=Q(r,z) \tag{38}$$

Note that the "source" term on the right-hand-side of the differential equation depends on frequency, Mach number, radius, and the z-dependence of the actuator velocity profile.

2.4 Derivation of the Non-Homogeneous Differential Equation in z

The solution to the non-homogeneous differential equation is obtained as an expansion in a series of eigenfunctions of the radial modes in an annular duct such that the expansion coefficients are functions of z that depend on mode order (m,n)

$$f(r,z) = \sum_{n=1}^{\infty} f_{mn}(z)\varphi_{mn}(\alpha_{mn}r) \tag{39}$$

where n is the radial mode index ordered such that the lowest order radial mode (the first) has n = 1, and the annular duct eigenfunctions are given by

$$\varphi_{mn}(\alpha_{mn}r) = J_m(\alpha_{mn}r) + C_{mn}Y_m(\alpha_{mn}r) \tag{40}$$

where J_m is the m^{th} order Bessel function of the first kind, and Y_m is the m^{th} order Bessel function of the second kind. The eigenvalues α_{mn} are the roots of the boundary condition equation for a hardwall annular duct,

$$\frac{\partial\varphi_{mn}(\alpha_{mn}r)}{\partial r} = 0 \qquad \text{at} \quad r = r_1 \quad \text{and} \quad r = r_2 \tag{41}$$

These roots can be found by various means, and are assumed to be known. Root-finding subroutines are provided as part of the program that implements this analysis for both cylindrical and annular ducts.

If we define

$$\gamma_{mn} \equiv \alpha_{mn}r_2 \tag{42}$$

then the mode coefficient C_{mn} can be written as

$$C_{mn} = \frac{-mJ_m(\gamma_{mn}) + \gamma_{mn}J_{m+1}(\gamma_{mn})}{mY_m(\gamma_{mn}) - \gamma_{mn}Y_{m+1}(\gamma_{mn})} \tag{43}$$

Note that if $r_1 = 0$, them $C_{mn} = 0$.

The first step in finding the unknown coefficients f_{mn} is to multiply through the differential equation (38) by $\varphi_{mn}r$ and integrate from r_1 to r_2.

$$\int_{r_1}^{r_2} \varphi_{mj}\mathcal{L}(f)rdr = \int_{r_1}^{r_2} Q(r,z)\varphi_{mj}(\alpha_{mj}r)rdr \tag{44}$$

Substituting Equation (39) for f in the differential operator, we have

$$\mathcal{L}(f) = \sum_{n=1}^{\infty} \mathcal{L}\left[f_{mn}(z)\varphi_{mn}(\alpha_{mn}r)\right] \tag{45}$$

Applying the differential operator to the individual terms in the sum, we get

$$\mathcal{L}[f_{mn}\varphi_{mn}] = f_{mn}\left[\frac{1}{r}\frac{\partial}{\partial r}\left(r\frac{\partial\varphi_{mn}}{\partial r}\right) - \frac{m^2\varphi_{mn}}{r^2} + k^2\varphi_{mn}\right] + 2ikM\frac{\partial f_{mn}}{\partial z}\varphi_{mn} +$$

$$\left(1-M^2\right)\frac{\partial^2 f_{mn}}{\partial z^2}\varphi_{mn} \tag{46}$$

The first two terms of the term in square brackets on the right-hand-side of Equation (46) can be recognized as the Bessel eigenfunction equation for the radial mode in a cylindrical or annular duct, so that we can (without proof) state the following relationship:

$$\frac{1}{r}\frac{\partial}{\partial r}\left(r\frac{\partial\varphi_{mn}}{\partial r}\right) - \frac{m^2\varphi_{mn}}{r^2} = -\alpha_{mn}^2\varphi_{mn} \tag{47}$$

Making these substitutions, Equation (44) becomes

$$\left(1-M^2\right)f''_{mj} + 2ikMf'_{mj} + \left(k^2 - \alpha_{mj}^2\right)f_{mj} = \frac{1}{N_{mj}}\int_{r_1}^{r_2} Q(r,z)\varphi_{mj}(\alpha_{mj}r)rdr \tag{48}$$

where

$$N_{mj} = \int_{r_1}^{r_2} \varphi_{mj}\varphi_{mj}rdr \tag{49}$$

is the mode normalization integral, where we have made use of the orthogonality properties of the eigenfunctions,

$$\int_{r_1}^{r_2} \varphi_{mn}\varphi_{mj} r dr = 0 \qquad \text{for} \quad n \neq j, \tag{50}$$

and where Q(r,z) is given by Equations (33) through (37).

The integration over r on the right-hand-side of Equation (48) breaks into four separate integrals, and can be written as

$$\int_{r_1}^{r_2} Q(r,z)\varphi_{mn}(\alpha_{mn} r) r dr = D_1(z)H_0^{mn} + D_2 H_1^{mn} + D_3 H_2^{mn} + D_4 H_3^{mn} \tag{51}$$

where

$$H_0^{mn} = \int_{r_1}^{r_2} \varphi_{mn}(\alpha_{mn} r) dr \tag{52}$$

$$H_1^{mn} = \int_{r_1}^{r_2} \varphi_{mn}(\alpha_{mn} r) r dr \tag{53}$$

$$H_2^{mn} = \int_{r_1}^{r_2} \varphi_{mn}(\alpha_{mn} r) r^2 dr \tag{54}$$

and

$$H_3^{mn} = \int_{r_1}^{r_2} \varphi_{mn}(\alpha_{mn} r) r^3 dr \tag{55}$$

These integrals must be calculated numerically, but will be constants depending only on mode order when computed. The integration subroutines are described briefly in Appendix A.

We now transform the differential equation in z to a form that explicitly shows the dependence on the actuator velocity function h(z) on the right-hand-side. The result is

$$\left(1-M^2\right)f''_{mj}+2ikMf'_{mj}+\left(k^2-\alpha^2_{mj}\right)f_{mj}=Q^{(1)}_{mn}h+Q^{(2)}_{mn}h'+Q^{(3)}_{mn}h'''+$$

$$Q^{(4)}_{mn}\frac{(h')^2}{h}+Q^{(5)}_{mn}\frac{h'h''}{h}+Q^{(6)}_{mn}\frac{(h'')^2}{h} \tag{56}$$

where

$$Q^{(1)}_{mn}=\left(m^2-1\right)BA_1H^{mn}_0+\left(4+m^2\right)BA_2H^{mn}_1-k^2BA_1H^{mn}_2-k^2BA_2H^{mn}_3 \tag{57}$$

$$Q^{(2)}_{mn}=\left(m^2-1\right)2i\frac{M}{k}BA_1H^{mn}_0+\left(4+m^2\right)2i\frac{M}{k}BA_2H^{mn}_1-4iMkBA_1H^{mn}_2-$$

$$4iMkBA_2H^{mn}_3 \tag{58}$$

$$Q^{(3)}_{mn}=-\left(m^2-1\right)\left(\frac{M}{k}\right)^2BA_1H^{mn}_0-\left(4+m^2\right)\left(\frac{M}{k}\right)^2BA_2H^{mn}_1-\left(1-2M^2\right)BA_1H^{mn}_2-$$

$$\left(1-2M^2\right)BA_2H^{mn}_3 \tag{59}$$

(60)

$$Q^{(4)}_{mn}=4M^2\left[BA_1H^{mn}_2-BA_2H^{mn}_3\right] \tag{61}$$

$$Q^{(5)}_{mn}=-\frac{2iM}{k}\left(1-2M^2\right)\left[BA_1H^{mn}_2-BA_2H^{mn}_3\right] \tag{62}$$

$$Q^{(6)}_{mn}=\frac{M^2\left(1-M^2\right)}{k^2}\left[BA_1H^{mn}_2-BA_2H^{mn}_3\right] \tag{63}$$

and where

$$BA_1=A_{2m}-\frac{A_{2m}-A_{1m}}{r_2-r_1}r_2 \tag{64}$$

$$BA_2 = \frac{A_{2m} - A_{1m}}{2(r_2 - r_1)} \tag{65}$$

The $Q_{mn}^{(j)}$ coefficients are constants, so that all the z-variation on the right-hand-side of Equation (56) is contained in the h-function and its derivatives. This completes the derivation of the ordinary differential non-homogeneous differential equation in z, which will now be solved.

2.5 Fourier Transform for z-Dependence

We solve Equation (56) using the method of infinite Fourier Transforms. Since we have not specified a particular form for the actuator velocity profile function h(z), we will only be able to express its Fourier transform symbolically at this point. The last three terms on the right-hand-side of Equation (56), which contain products and ratios of the h-function and its derivatives, are particularly troublesome.

The Fourier Transform of the f-function will be written as

$$F(\kappa) \equiv \mathcal{F}[f(z)] = \int_{-\infty}^{\infty} f(z) e^{+i\kappa z} dz \tag{66}$$

The relationships for the Fourier Transform of derivatives of the f-function are

$$\mathcal{F}[f'(z)] = -i\kappa F(\kappa) \tag{67}$$

and

$$\mathcal{F}[f''(z)] = -\kappa^2 F(\kappa) \tag{68}$$

and the inverse transform is defined as

$$f(z) = \frac{1}{2\pi} \int_{-\infty}^{\infty} e^{-i\kappa z} F(\kappa) d\kappa \tag{69}$$

Note that this form of the Fourier Transform pair is the complex conjugate of that found in many reference works. The choice of sign on the exponent in the integrand is arbitrary.

We will denote the Fourier Transform of the h-function as

$$\mathcal{H}(\kappa) = \mathcal{F}[h(z)]$$

Taking the Fourier Transform of Equation (56), using the relationships for Fourier Transforms of derivatives, and solving for the Fourier Transform of f_{mn}, we get

$$F_{mn}(\kappa) = \frac{\left[Q_{mn}^{(1)} - i\kappa Q_{mn}^{(2)} - \kappa^2 Q_{mn}^{(3)}\right]\mathcal{H}(\kappa) + Q_{mn}^{(4)}H_4 + Q_{mn}^{(5)}H_5 + Q_{mn}^{(6)}H_6}{\left[\left(k^2 - \alpha_{mn}^2\right) + 2kM\kappa - \left(1 - M^2\right)\kappa^2\right]} \tag{70}$$

where H_4, H_5, and H_6 are the Fourier Transforms of the functions involving ratios of h(z), defined as

$$H_4 = \mathcal{F}\left(\frac{h'^2}{h}\right) \tag{71}$$

$$H_5 = \mathcal{F}\left(\frac{h'h''}{h}\right) \tag{72}$$

and

$$H_6 = \mathcal{F}\left(\frac{h''^2}{h}\right) \tag{73}$$

There are six inversion integrals to be evaluated:

$$G_1(z) = \frac{1}{2\pi}\int_{-\infty}^{\infty} \frac{Q_{mn}^{(1)}\mathcal{H}(\kappa)e^{-i\kappa z}}{\left(k^2 - \alpha_{mn}^2\right) + 2kM\kappa - \left(1 - M^2\right)\kappa^2} d\kappa \tag{74}$$

$$G_2(z) = \frac{1}{2\pi}\int_{-\infty}^{\infty} \frac{-i\kappa Q_{mn}^{(2)}\mathcal{H}(\kappa)e^{-i\kappa z}}{\left(k^2 - \alpha_{mn}^2\right) + 2kM\kappa - \left(1 - M^2\right)\kappa^2} d\kappa \tag{75}$$

$$G_3(z) = \frac{1}{2\pi}\int_{-\infty}^{\infty} \frac{-\kappa^2 Q_{mn}^{(3)}\mathcal{H}(\kappa)e^{-i\kappa z}}{\left(k^2 - \alpha_{mn}^2\right) + 2kM\kappa - \left(1 - M^2\right)\kappa^2} d\kappa \tag{76}$$

$$G_4(z) = \frac{1}{2\pi}\int_{-\infty}^{\infty} \frac{Q_{mn}^{(4)}H_4(\kappa)e^{-i\kappa z}}{\left(k^2 - \alpha_{mn}^2\right) + 2kM\kappa - \left(1 - M^2\right)\kappa^2} d\kappa \tag{77}$$

$$G_5(z) = \frac{1}{2\pi}\int_{-\infty}^{\infty} \frac{Q_{mn}^{(5)} H_5(\kappa) e^{-i\kappa z}}{\left(k^2 - \alpha_{mn}^2\right) + 2kM\kappa - \left(1 - M^2\right)\kappa^2} d\kappa \tag{78}$$

and

$$G_6(z) = \frac{1}{2\pi}\int_{-\infty}^{\infty} \frac{Q_{mn}^{(6)} H_6(\kappa) e^{-i\kappa z}}{\left(k^2 - \alpha_{mn}^2\right) + 2kM\kappa - \left(1 - M^2\right)\kappa^2} d\kappa \tag{79}$$

The first three integrals will be evaluated using the residue theorem, and the last three integrals will be shown to take simple forms for the particular form of h(z) chosen.

To apply the residue theorem, we need to find the roots in the denominator of the integrand, which is the same in all the integrals. We assume that the Fourier transform of h(z) possesses no singularities so that all the roots are obtained from the denominator,

$$-\left(1 - M^2\right)\kappa^2 + 2kM\kappa + \left(k^2 - \alpha_{mn}^2\right) = 0 \tag{80}$$

There are two values of κ that satisfy this relationship:

$$\kappa^{\binom{1}{2}} = \frac{-kM \pm \sqrt{k^2 - \left(1 - M^2\right)\alpha_{mn}^2}}{1 - M^2} \tag{81}$$

These can be identified as the axial propagation constants for forward and backward traveling waves in a duct with uniform flow. In terms of the two roots, we can write the denominator of the integrand as

$$\left(1 - M^2\right)\kappa^2 - 2kM\kappa - \left(k^2 - \alpha_{mn}^2\right) = -\left(1 - M^2\right)\left(\kappa - \kappa^{(1)}\right)\left(\kappa - \kappa^{(2)}\right) \tag{82}$$

Substituting this into Equation (74) for $G_1(z)$ gives

$$G_1(z) = -\frac{Q_1}{2\pi\left(1 - M^2\right)}\int_{-\infty}^{\infty} \frac{\mathcal{H}(\kappa) e^{-i\kappa z} dz}{\left(\kappa - \kappa^{(1)}\right)\left(\kappa - \kappa^{(2)}\right)} \tag{83}$$

The inverse Fourier Transform can be evaluated in this case using the residue theorem, and the method is considered in detail in Appendix B. The solution for the forward-traveling (m,n) mode can be shown to be

$$G_1(z) = -\frac{iQ_{mn}^{(1)}}{2}\frac{\mathcal{H}\left(-\kappa_{mn}^{+}\right)e^{i\kappa_{mn}^{+}z}}{\sqrt{k^2-\left(1-M^2\right)\alpha_{mn}^2}} \tag{84}$$

where

$$\kappa_{mn}^{+} = \frac{-kM+\sqrt{k^2-\left(1-M^2\right)\alpha_{mn}^2}}{1-M^2} \tag{85}$$

is the axial propagation constant for the forward-propagating (m,n) mode.

Similarly, the solutions for G_2 and G_3 can be obtained as

$$G_2(z) = -\kappa_{mn}^{+}Q_{mn}^{(2)}\frac{\mathcal{H}\left(-\kappa_{mn}^{+}\right)e^{i\kappa_{mn}^{+}z}}{\sqrt{k^2-\left(1-M^2\right)\alpha_{mn}^2}} \tag{86}$$

and

$$G_3(z) = i\left(\kappa_{mn}^{+}\right)^2 Q_{mn}^{(3)}\frac{\mathcal{H}\left(-\kappa_{mn}^{+}\right)e^{i\kappa_{mn}^{+}z}}{\sqrt{k^2-\left(1-M^2\right)\alpha_{mn}^2}} \tag{87}$$

We can evaluate the G_4, G_5, and G_6 functions if we make some restrictions on the form of the ratios of h-functions and derivatives in H_4, H_5, and H_6. If we require that H_4, H_5, and H_6 have no poles to contribute to the residues within the contour of integration, the solution for the G_4, G_5, and G_6 functions can be written in terms of H_4, H_5, and H_6 as

$$G_4(z) = -\frac{iQ_{mn}^{(4)}}{2}\frac{H_4\left(-\kappa_{mn}^{+}\right)e^{i\kappa_{mn}^{+}z}}{\sqrt{k^2-\left(1-M^2\right)\alpha_{mn}^2}} \tag{88}$$

$$G_5(z) = -\frac{iQ_{mn}^{(5)}}{2}\frac{H_5\left(-\kappa_{mn}^{+}\right)e^{i\kappa_{mn}^{+}z}}{\sqrt{k^2-\left(1-M^2\right)\alpha_{mn}^2}} \tag{89}$$

and

$$G_6(z) = -\frac{iQ_{mn}^{(6)}}{2}\frac{H_6\left(-\kappa_{mn}^{+}\right)e^{i\kappa_{mn}^{+}z}}{\sqrt{k^2-\left(1-M^2\right)\alpha_{mn}^2}} \tag{90}$$

To derive these inverse Fourier transformations, we have had to apply restrictions on the form of the actuator velocity z-dependence. We require that the Fourier transform of h(z) have no poles in the lower half plane (see Appendix B), and that the Fourier transforms of the derivative ratio functions also have no poles in the lower half plane. Without these restrictions, it is necessary to return to the original Fourier Transform integrals, which may be very difficult to evaluate.

2.6 Solution for the Acoustic Pressure Field Generated by the Actuators

The (m,n) mode contribution for the f-function that was used to transform the differential equation and boundary conditions has been determined and can be written

$$f_{mn}(z) = \mathcal{F}^{-1}\left[F_{mn}(\kappa)\right] = G_1 + G_2 + G_3 + G_4 + G_5 + G_6 \tag{91}$$

writing out the G-terms, this becomes

$$f_{mn}(z) = \left[-\frac{iQ_{mn}^{(1)}}{2} - \kappa_{mn}^{+}Q_{mn}^{(2)} + i\left(\kappa_{mn}^{+}\right)^2 Q_{mn}^{(3)}\right]\frac{\mathcal{H}\left(-\kappa_{mn}^{+}\right)e^{i\kappa_{mn}^{+}z}}{\sqrt{k^2-\left(1-M^2\right)\alpha_{mn}^2}}$$

$$-\frac{i}{2}\left[Q_{mn}^{(4)}H_4\left(-\kappa_{mn}^{+}\right) + Q_{mn}^{(5)}H_5\left(-\kappa_{mn}^{+}\right) + Q_{mn}^{(5)}H_5\left(-\kappa_{mn}^{+}\right)\right]\frac{e^{i\kappa_{mn}^{+}z}}{\sqrt{k^2-\left(1-M^2\right)\alpha_{mn}^2}} \tag{92}$$

Then, combining Equations (21), (22), and (39), we can express the pressure field in the m^{th} order spinning mode generated by the wall-mounted inner and outer actuator ring source as

$$p(r,\theta,z) = \left\{\sum_{n=1}^{\infty}\left[f_{mn}(z)\varphi_{mn}(\alpha_{mn}r)\right] + \left[B_1(z)r + 2B_2(z)r^2\right]h(z)\right\}e^{im\theta} \tag{93}$$

The only unknown left to make this a computable formula is the Fourier Transform of the actuator velocity profile in z. This, of course, depends upon the choice of function used to represent the piston vibration, and will be solved for the particular case of a box function in the next section.

3. Solution for Box Function Actuator

3.1 Choice of Box Function Actuator Velocity Profile

Several choices present themselves for the shape of the axial velocity profile for the actuator motion, h(z). The preferred choice will have a known and acceptable Fourier transform and will furthermore have a simple Fourier Transform for the three ratio functions involving h(z) and its first and second derivatives. It is assumed that the circumferential velocity profile has already been accounted for in the spinning mode decomposition.

Three more obvious possibilities are:

1. Delta function source - zero axial length but finite volume velocity
2. Box function source - rigid piston motion with a displacement and velocity discontinuity at the edges
3. Half-sine-wave source - good representation of the lowest simply-supported plate vibration mode, displacement and velocity go to zero at the edges.

The Fourier Transform of the delta function is well known, but some difficulty may be encountered in finding the transforms of combinations like

$$\mathcal{F}\left(\frac{\delta'(z)^2}{\delta(z)}\right),\ \mathcal{F}\left(\frac{\delta'(z)\delta''(z)}{\delta(z)}\right),\ \text{and}\ \mathcal{F}\left(\frac{\delta''(z)^2}{\delta(z)}\right)$$

Also, a function of finite extent may be a better physical representation of the actuator for the shorter modal axial wavelengths. For these reasons, the delta function was not considered at this time.

The box function, as illustrated in Figure (2) has a constant velocity amplitude between $0 \le z \le L$, and represents the motion of a rigid piston actuator. The Fourier Transform of this function is given by

$$\mathcal{F}(-\kappa) = \frac{1}{\sqrt{2\pi}} \frac{e^{-i\kappa L} - 1}{-i\kappa} \tag{94}$$

Since the first and second derivatives of h(z) are zero (neglecting edge effects), we have

$$H_4 = H_5 = H_6 = 0 \tag{95}$$

This is the velocity function used for further illustration by a sample calculation. The box function could be an approximate representation of a source of any other shape

by choosing the velocity of the piston based on an effective volume velocity for the more complex actuator.

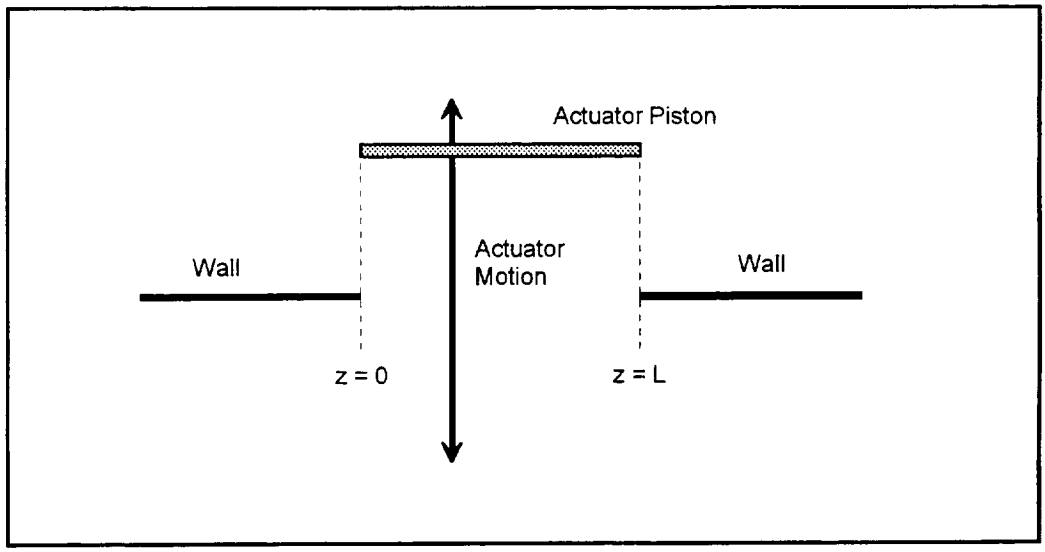

Figure (2) Diagram of box function axial velocity profile for actuator.

The very realistic half-sine-wave velocity profile has an easily calculated Fourier transform, but the transform of the ratio functions may take some additional effort. Examination of this case is left for the future, and is recommended as a follow-on task.

3.2 Sample Computations for Box Function Case

The computer program FDANC has been written to compute the acoustic pressure coupling of wall-mounted rings of ANC actuators in cylindrical or annular ducts. The program was used to compute the modes generated in the inlet and exhaust ducts of an analytical model that simulates the NASA ANC Fan that is mounted in the NASA Lewis AAPL Test Facility. The parameters that are held constant throughout the computations are the following:

Inlet and Exhaust outer radius = 2.0 feet
Exhaust inner radius = 0.6145 feet
Flow temperature = 70 degF
Spinning mode order, m = 6
Number of radial modes = 6
Outer wall SPL = 110 dB
Axial length of ANC actuator = 4.5 inches

For this study, both cylindrical and annular ducts were considered, using the above parameters. Two values of mean flow Mach number were used, Mach 0.0 and 0.1. The

annular duct case was run with actuators on the outer wall only, inner wall only, and both walls. For the cases with actuators on both the inner an outer walls, the inner wall actuator velocity was set to a value based on the ratio of the first radial mode shape at the inner wall to that at the outer wall. Two cases with a higher radius ratio ($R_1/R_2 = 0.75$) were compared. Finally, a case at a higher frequency with two cut-on radial modes is presented. A brief outline of the differences among the cases is presented in Table (1):

Table (1) Differences among sample cases used for computations. All cases have same outer radius ($R_2 = 2.0$) and same spinning mode order (m = 6).

Case Number	Inner Radius R_1, ft.	Mach Number	Frequency Hz.	Inner Actuator Active?	Outer Actuator Active?
1	0.0	0.0	935	n/a	Yes
2	0.6146	0.0	935	No	Yes
3	0.0	0.1	935	n/a	Yes
4	0.6146	0.1	935	No	Yes
5	0.6146	0.1	935	Yes	No
6	0.6146	0.1	935	Yes	Yes
7	1.5	0.1	935	No	Yes
8	1.5	0.1	935	Yes	Yes
9	1.5	0.1	1350	Yes	Yes

3.2.1 Computer Output for Case 1, Cylindrical Duct, Mach 0.0, m = 6

This is a basic run for the inlet duct to illustrate the program output. This case has no mean flow, and the frequency is such that only one radial mode is cut-on for the m = 6 spinning mode. The results will be compared below to a flow case.

```
                PROGRAM FDANC1 - TURBOFAN ANC SPECS

          CYLINDRICAL OR ANNULAR HARDWALL DUCT ROOTS FOUND AS
           ROOTS OF DERIVATIVE OF BESSEL FUNCTION

 INNER RAD =      .000  OUTER RAD =    2.000 DUCT HGT =    2.000 ft

    DUCT MACH # =      .00000
    FLOW TEMPERATURE =    70.00000 deg F
    SPEED OF SOUND =    1128.295 ft/sec    343.904 m/sec
    FREQUENCY =     935.0 Hz., ETA =    1.65737
    WAVE NUMBER, k =    17.08260  per m., kH =   10.41355
    SPL =     110.000 dB
    AXIAL LENGTH OF ANC PORT =      4.500000 in.
    AIR DENSITY =    1.2300E+00 kg/m^3
    RHO*CS =      423.0023 MKS Rayls

SPINNING MODE ORDER, m =    6
NUMBER OF RADIAL MODES =    6

    THIS DUCT TAKEN AS CYLINDRICAL WITH INNER RADIUS SET TO 0

 JR      HW ROOT          PROP CNST (RE,IM)     CUT-OFF FRQ    HW COR  AXL WVLNTH   MOD ANG
        ALPHA*R2                PER METER            HZ                    ft        deg

  1     7.501266      11.848900      .000000     673.515      1.39       .5303     46.08
  2    11.734940        .000000     8.874456    1053.643       .89       .0000     90.00
  3    15.268180       -.000001    18.316620    1370.882       .68       .0000     90.00
  4    18.637440       -.000001    25.355620    1673.397       .56       .0000     90.00
```

```
 5    21.931720       -.000001    31.663000    1969.180       .47        .0000      90.00
 6    25.183930       -.000002    37.614940    2261.186       .41        .0000      90.00

   PRESSURE AT SPL =      6.3246E+00 nt/m^2
   ENERGY IN J=1 MODE =      2.7583E-02 watts
   DESIRED MODE AMPLITUDE =      1.7859E+01 nt/m^2

INITIAL PISTON VELOCITY, INNER WALL =       .000000      .000000 m/sec
INITIAL PISTON VELOCITY, OUTER WALL =      1.000000      .000000 m/sec
INNER VELOC/OUTER VELOC =       .000000      .000000

 JR      EV-ALPHA              MODE C-VAL              MODE COEFF (RE,IM)      MAG MODE AMPL
        PER METER                                          nt/m^2                  nt/m^2

  1    12.305230       .000000     .000000       1.785888E+01   -1.561900E-07     1.7859E+01
  2    19.250220       .000000     .000000       1.535435E-01    1.909916E-01     2.4506E-01
  3    25.046230       .000000     .000000       1.788268E-01    2.224413E-01     2.8541E-01
  4    30.573230       .000000     .000000       7.065713E-02    8.788983E-02     1.1277E-01
  5    35.977220       .000000     .000000       8.507293E-02    1.058215E-01     1.3578E-01
  6    41.312210       .000000     .000000       1.325678E-02    1.649000E-02     2.1158E-02

   VELOCITY AT INNER WALL =     0.00000E+00   0.00000E+00 m/s
   VELOCITY AT OUTER WALL =    -5.77585E-02   4.64337E-02 m/s
   DISPLACEMENT AMPLITUDE, INNER WALL =     0.00000E+00 in
   DISPLACEMENT AMPLITUDE, OUTER WALL =     4.96668E-04 in.
```

It should be noted that the values in the column marked "HW ROOT" are the roots of the Bessel function boundary condition, γ_{mj}, which are nondimensional, but that the value in the column marked "EV-ALPHA" are the α_{mj}, in dimensions of 1/meters. The propagation constants are also in units of 1/meters. The MODE C-VAL is the coefficient that multiplies the Bessel function of the second kind in the annular duct eigenfunction, and thus is zero for the cylindrical duct eigenfunction. The columns marked MODE COEFF (RE, IM) are the complex mode coefficients for the pressure solution, and are the desired results of the computation.

Note that the desired mode amplitude to achieve 110 dB SPL in the first radial mode (the only cut-on mode) requires a pressure amplitude of 6.32 nt/m^2 at the outer wall and a mode coefficient amplitude of 17.86 nt/m^2. The displacement amplitude that is required for the actuators to generate this mode coefficient is 5.0×10^{-4} in.

The magnitudes of the mode coefficients for this case are plotted in Figure (3), and the pressure profile is shown in Figure (4). Note that the second highest mode, the third, is 36 dB down from the first mode, indicating excellent coupling to the cut-on mode for this case. The pressure profile is essentially the pure m = 6, j = 1 Bessel function of the first kind.

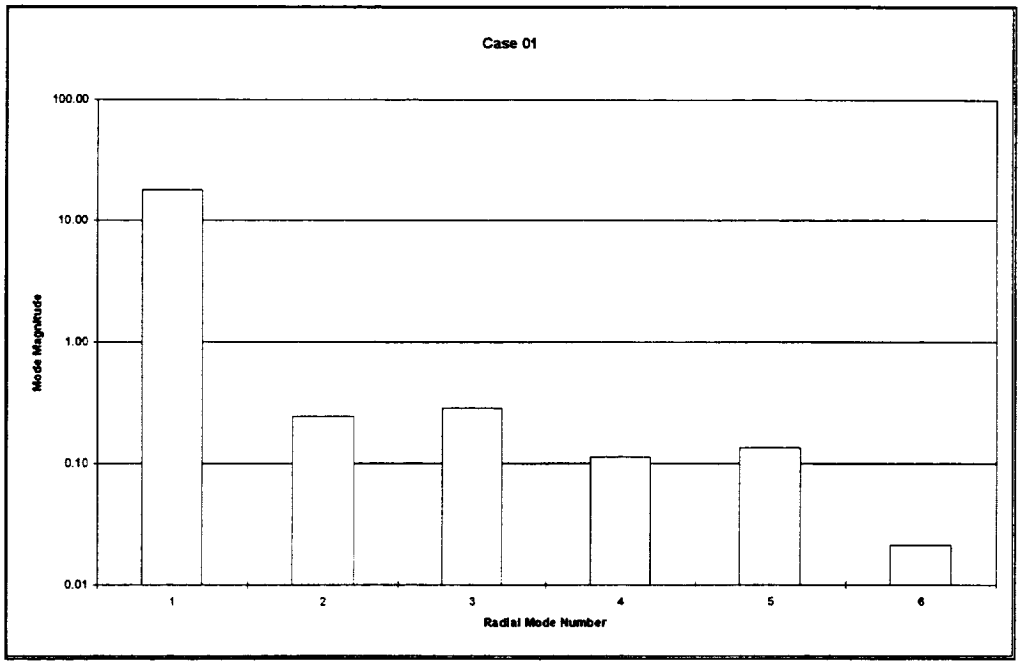

Figure (3) Mode coefficients for Case 1

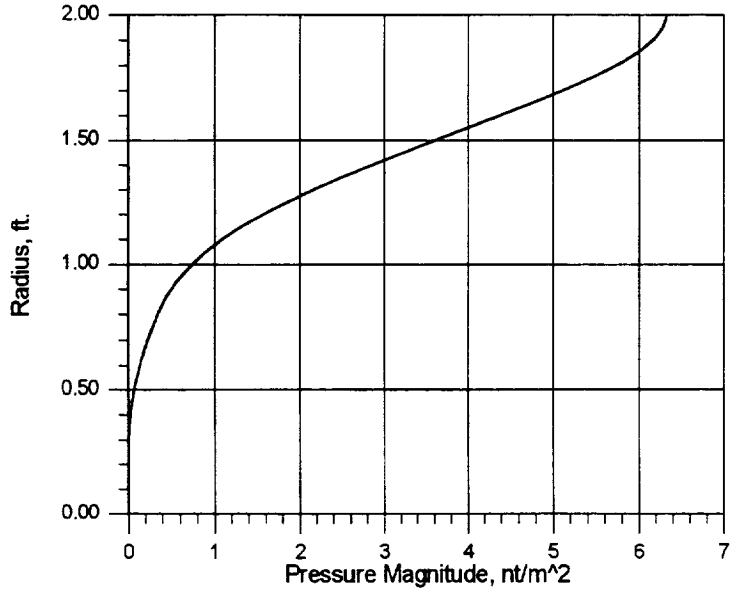

Figure (4) Pressure profile for Case 1

3.2.2 Computer Output for Case 2, Annular Duct, Mach 0.0, m = 6, Outer Wall Actuator Only

This case is for the annular duct with no flow, with a radius ratio of 0.307. The actuator velocity at the inner wall in this case is set equal to zero. The output for the annular duct case is slightly different, and is shown below:

```
              PROGRAM FDANC1 - TURBOFAN ANC SPECS

         CYLINDRICAL OR ANNULAR HARDWALL DUCT ROOTS FOUND AS
          ROOTS OF DERIVATIVE OF BESSEL FUNCTION

 INNER RAD =      .615  OUTER RAD =    2.000 DUCT HGT =    1.385 ft

    DUCT MACH # =      .00000
    FLOW TEMPERATURE =    70.00000 deg F
    SPEED OF SOUND =    1128.295 ft/sec    343.904 m/sec
    FREQUENCY =     935.0 Hz., ETA =    1.14806
    WAVE NUMBER, k =    17.08260  per m., kH =    7.21347
    SPL =     110.000 dB
    AXIAL LENGTH OF ANC PORT =     4.500000 in.
    AIR DENSITY =    1.2300E+00 kg/m^3
    RHO*CS =      423.0023 MKS Rayls

SPINNING MODE ORDER, m =    6
NUMBER OF RADIAL MODES =    6

    ANNULAR DUCT ANALYSIS USED

  J          GREC          GCYL          GANN

  1         .0000        7.5013        7.5010
  2        4.5353       11.7349       11.7178
  3        9.0706       15.2682       15.1073
  4       13.6059       18.6374       18.1882
  5       18.1411       21.9317       21.5424
  6       22.6764       25.1839       25.3502

 JR      HW ROOT          PROP CNST (RE,IM)    CUT-OFF FRQ    HW COR  AXL WVLNTH   MOD ANG
        ALPHA*R2                PER METER            HZ                    ft        deg

  1     7.501023      11.849320      .000000     673.493      1.39       .5303     46.08
  2    11.717810       .000000     8.813345    1052.105       .89       .0000     90.00
  3    15.107290      -.000001    17.954040    1356.436       .69       .0000     90.00
  4    18.188200      -.000001    24.461990    1633.061       .57       .0000     90.00
  5    21.542440      -.000001    30.935500    1934.228       .48       .0000     90.00
  6    25.350170      -.000002    37.914260    2276.112       .41       .0000     90.00

    PRESSURE AT SPL =     6.3246E+00 nt/m^2
    ENERGY IN J=1 MODE =     2.7591E-02 watts
    DESIRED MODE AMPLITUDE =     1.7859E+01 nt/m^2

 INITIAL PISTON VELOCITY, INNER WALL =      .000000     .000000 m/sec
 INITIAL PISTON VELOCITY, OUTER WALL =     1.000000     .000000 m/sec
 INNER VELOC/OUTER VELOC =      .000000     .000000

  JR      EV-ALPHA              MODE C-VAL              MODE COEFF (RE,IM)     MAG MODE AMPL
         PER METER                                          nt/m^2                nt/m^2

   1    12.304830     -.000129     .000000      1.785888E+01   -1.703681E-07    1.7859E+01
   2    19.222130     -.014592     .000000      6.858777E-01    8.531162E-01    1.0946E+00
   3    24.782310     -.148402     .000000      6.013200E-02    7.479410E-02    9.5969E-02
   4    29.836290     -.451348     .000000     -7.545694E-02   -9.385574E-02    1.2043E-01
   5    35.338650     -.392167     .000000      2.288906E-02    2.847013E-02    3.6530E-02
   6    41.584930      .162785     .000000     -4.326065E-02   -5.380896E-02    6.9043E-02

    VELOCITY AT INNER WALL =    0.00000E+00   0.00000E+00 m/s
    VELOCITY AT OUTER WALL =   -7.17790E-02   5.77080E-02 m/s
    DISPLACEMENT AMPLITUDE, INNER WALL =    0.00000E+00 in
    DISPLACEMENT AMPLITUDE, OUTER WALL =    6.17243E-04 in.
```

Figure (5) shows the mode coefficient magnitude for this case, and Figure (6) shows the pressure profile. Note that the second radial mode is 24 dB down from the first mode in this case, indicating very good coupling efficiency. An actuator displacement amplitude of 6.2×10^{-4} inches is required to achieve the required SPL level. Generally, the case is very similar to the cylindrical duct case, as one might expect at this low radius ratio.

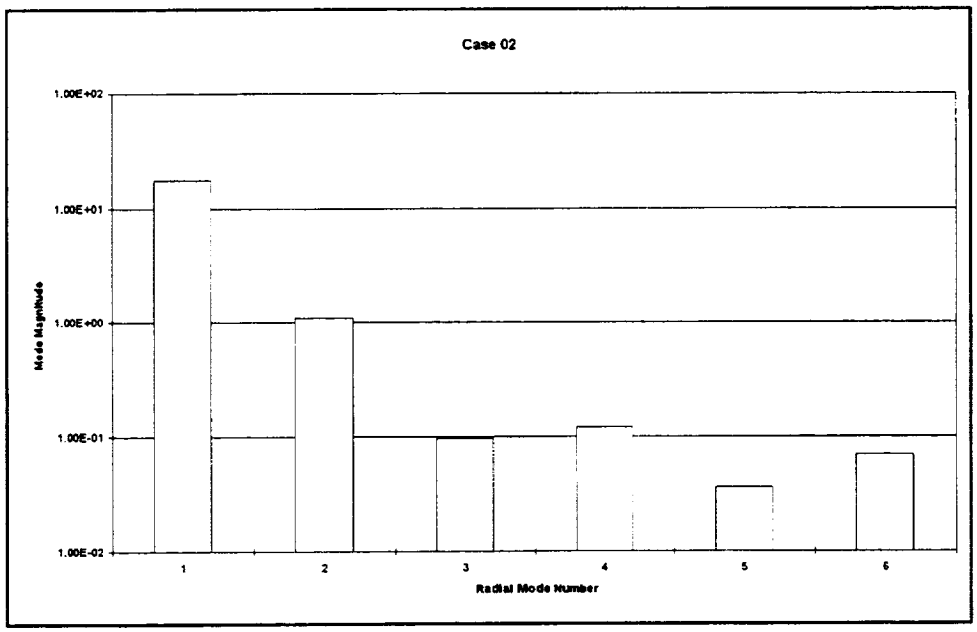

Figure (5) Mode coefficients for Case 2

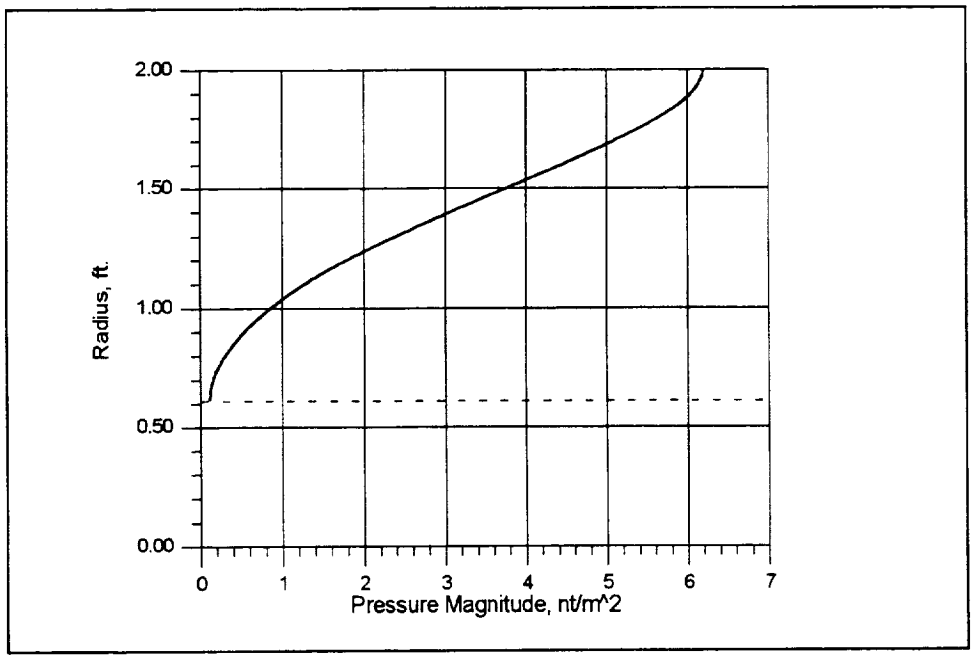

Figure (6) Pressure profile for Case 2

3.2.3 Comparison of Cases 1 and 3

Cases 1 and 3 are for the cylindrical duct, Case 1 with no flow and Case 3 with a flow Mach number of 0.1. The mean flow of Mach 0.1 has had very little effect on the mode coupling due to the actuator in this case, as can be seen from Figure (7), which compares the mode magnitudes for the cases with and without flow. The pressure profiles are nearly indistinguishable from those presented previously.

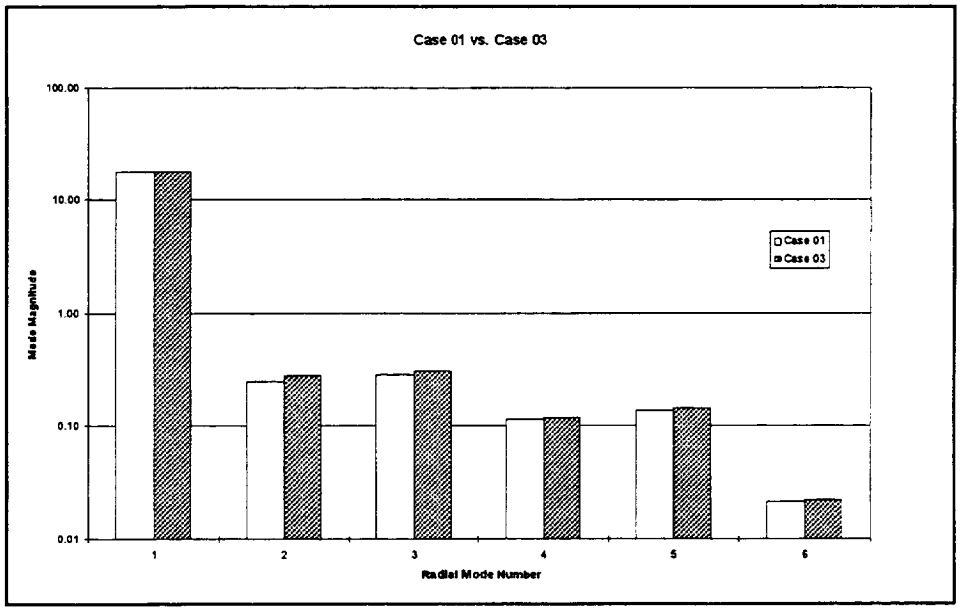

Figure (7) Mode coefficients for Case 3 compared to coefficients for Case 1.

3.2.4 Comparison of Cases 2 and 4

Cases 2 and 4 compare the annular duct with and without flow. Case 4 is the baseline case for the annular duct with the actuator active on the outer wall only, with Mach 0.1 flow. As in the cylindrical duct case, the mean flow of Mach 0.1 has had little effect. Figure (8) compares the modes generated by the actuator for Case 2 (no-flow) and Case 4 (Mach 0.1). The pressure profiles are nearly indistinguishable from those presented previously.

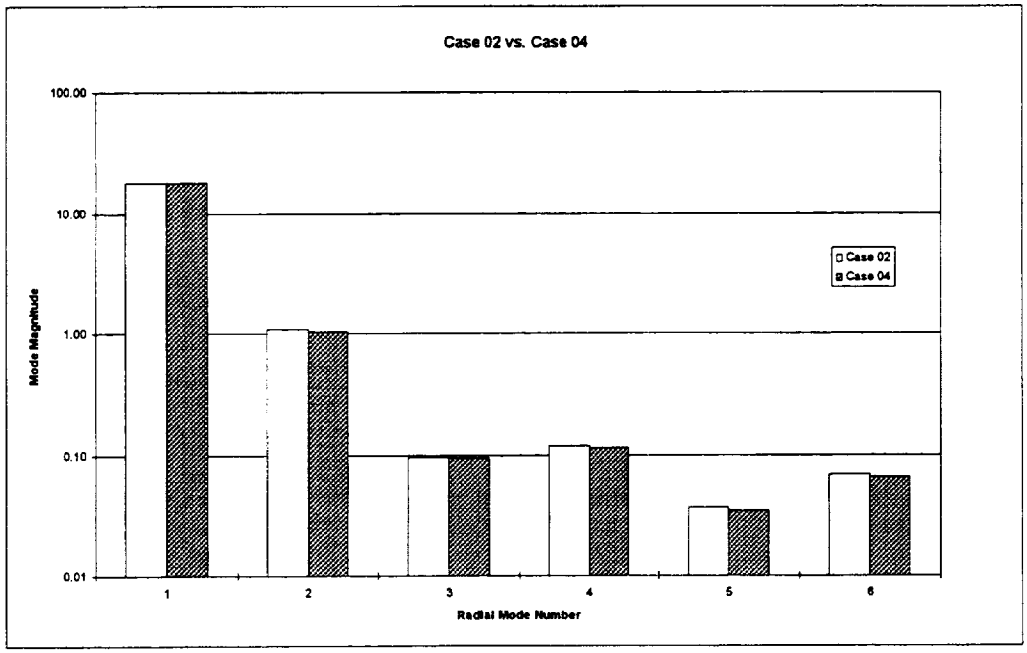

Figure (8) Comparison of mode coefficients for Cases 2 and 4.

3.2.5 Comparison of Cases 4 and 5

In Case 5, only the inner wall of actuators is active, otherwise the conditions are the same as for Case 4. Figure (9) compares the generated mode magnitudes for Cases 4 and 5, and indicates that the actuators at the inner wall only tend to generate higher output in the higher order modes, an indication of reduced coupling efficiency. The second mode is 14.7 dB down in Case 5, compared to 24.7 dB down in Case 4. Figure (10) shows the slightly different pressure profile obtained from the inner wall actuator case.

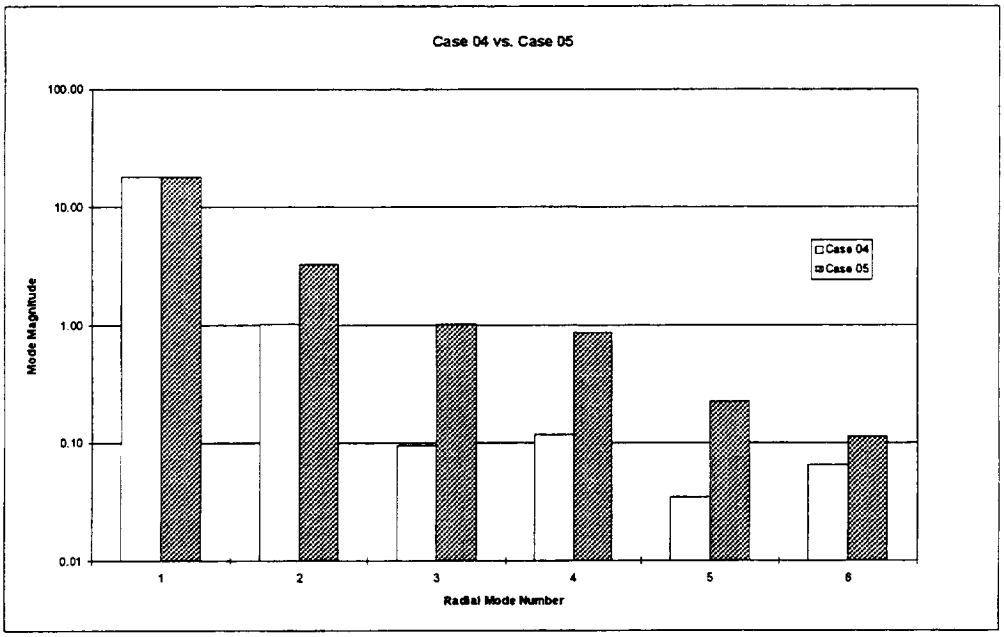

Figure (9) Comparison of mode coefficients for Cases 4 and 5.

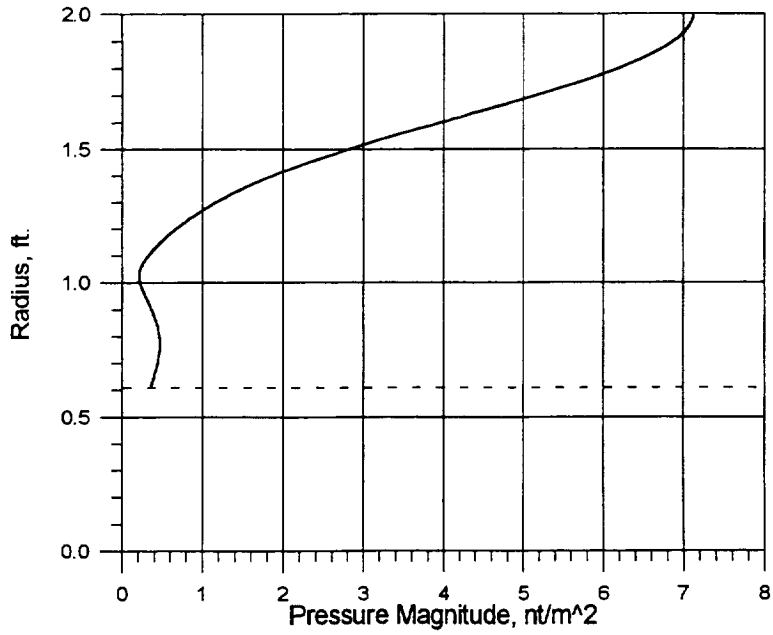

Figure (10) Pressure profile for Case 5

3.2.6 Comparison of Cases 4 and 6

In Case 6, both inner and outer actuators are active. It is necessary to choose the relative magnitude and phase of the velocity for the inner actuators for input to the

problem. The objective is to choose the magnitude and phase of the inner actuators such that the combination of actuators gives the least amount of amplitude to the higher order modes, coupling most efficiently to the cut-on mode. There is no direct method of deriving this inner actuator velocity a priori (one would have to use the analysis developed in this study in the *backward* sense, rather than the forward sense of predicting what pressure modes couple to a given actuator motion).

As a first estimate, the inner actuator velocity was set to a magnitude and phase determined by the ratio of the pressure first mode eigenfunction at the inner radius to the pressure at the outer surface, assuming the velocities might have roughly the same ratio. The inner to outer radius pressure ratio was determined to be 0.015432 + 0.0i.

Figure (11) compares the mode coefficients for these two cases, and indicates that there is not much difference. The radius ratio in this case, however, is quite low, at 0.31, so that the velocity at the inner actuator is quite small. There may be some other value of inner wall actuator velocity that offers some improvement in coupling efficiency, but it would have to be sought by trial and error.

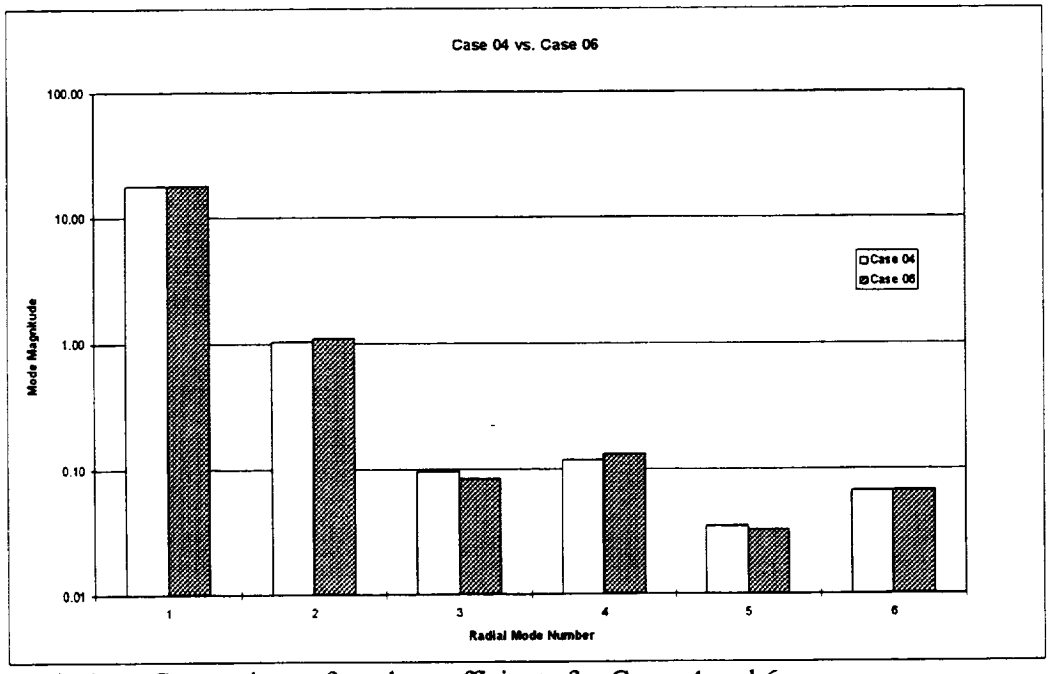

Figure (11) Comparison of mode coefficients for Cases 4 and 6

3.2.7 Comparison of Cases 7 and 8

For Cases 7 and 8 the inner radius was increased to 1.5 feet, giving an annular duct radius ratio of 0.75. In Case 7, only the outer wall actuator is activated. In Case 8, both inner and outer wall actuators are activated, and the ratio of inner wall actuator velocity to

outer wall is determined using the same method described in Case 6. Figure (12) shows the comparison of mode coefficients for Cases 7 and 8.

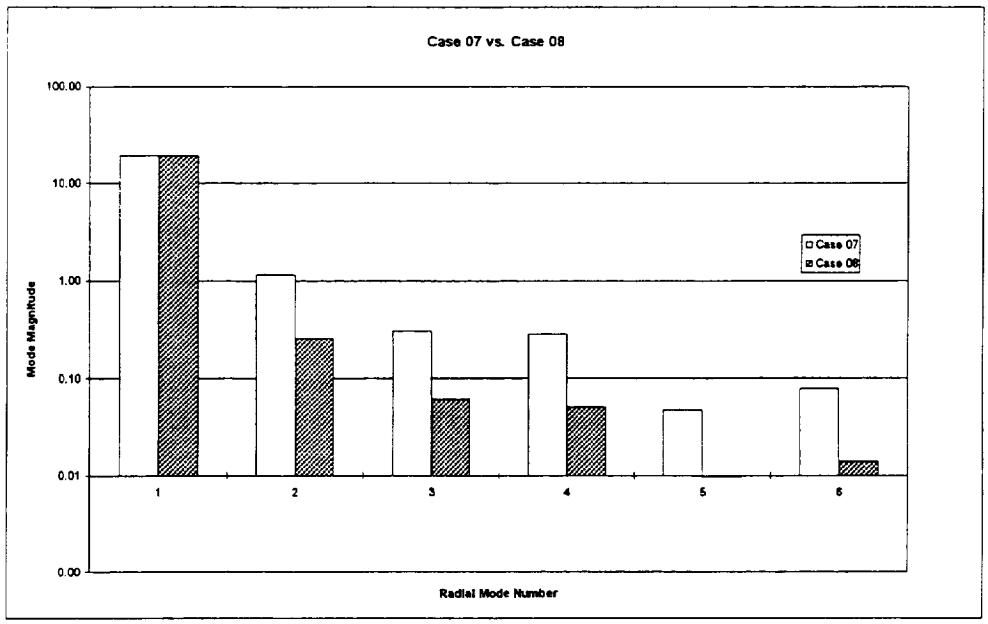

Figure (12) Comparison of mode coefficients for Cases 7 and 8

In this case, a marked improvement of coupling efficiency is noted. The second radial mode is 24.3 dB down in Case 7 with outer wall actuators only, but the second radial is 37 dB down for Case 8, for this particular choice of inner wall actuator velocity. Although this may not be the optimum coupling efficiency, it does indicate the potential for improved coupling to a single mode using both inner and outer actuator rings.

The pressure profiles are almost identical in these cases, since the only difference is in the higher order mode content, which is small for both cases. It should be noted that the substantial 24 dB difference obtained with the outer wall actuator ring only may make the additional expense of an inner actuator ring unnecessary. It would certainly seem to be unwise for the low radius ratio case. This would have to be evaluated on a case-by-case basis.

3.2.8 Discussion of Case 9

Although the computer program is aimed primarily at the case in which only one radial mode is cut on, for which it calculates the "spillover" into cut-off modes, it will calculate the radial mode coupling independently of the number of cut-on radial modes. It is not obvious, however, how to choose the inner wall actuator velocity relative to the outer wall actuator velocity to best couple to two radial modes, which will have relative magnitudes and phases. It is not clear at this point whether the two coplanar actuator rings can be used to generate two independent radial modes.

As an example of a case with two cut on radial modes, Case 9 increases the frequency of Case 8 to 1350 Hz. The mode coefficients of the fan noise source are assumed to be the following values at the actuator source plane (assuming these modes are the anti-phase values):

$A_1 = 1.0 + 0.0\,i$
$A_2 = 0.5 - 0.2i$

This is the source that the ANC actuator system must try to match. The difficulty is to determine the inner wall actuator velocity (relative to the outer wall), that will best match these two modes.

In an actual ANC system with feedback control sensors, the inner and outer wall actuator velocities in the m = 6 mode would be adjusted (in somewhat of a trial-and-error process) by the control system to values that attempt to achieve cancellation. A key question is whether such a set of control parameters exist, because this will bear directly on the stability of the control system operation.

In this case, a first guess at the inner wall velocity was made by computing the ratio of the pressure of the sum of the two fan source modes at the inner wall to the pressure of the sum of the two fan source modes at the outer wall. The following is the output run for this case:

```
              PROGRAM FDANC1 - TURBOFAN ANC SPECS

          CYLINDRICAL OR ANNULAR HARDWALL DUCT ROOTS FOUND AS
           ROOTS OF DERIVATIVE OF BESSEL FUNCTION

 INNER RAD =    1.500  OUTER RAD =    2.000 DUCT HGT =     .500 ft

    DUCT MACH # =      .10000
    FLOW TEMPERATURE =    70.00000 deg F
    SPEED OF SOUND =   1128.295 ft/sec    343.904 m/sec
    FREQUENCY =   1350.0 Hz., ETA =      .59825
    WAVE NUMBER, k =   24.66471  per m., kH =    3.75890
    SPL =    110.000 dB
    AXIAL LENGTH OF ANC PORT =     4.500000 in.
    AIR DENSITY =   1.2300E+00 kg/m^3
    RHO*CS =     423.0023 MKS Rayls

SPINNING MODE ORDER, m =   6
NUMBER OF RADIAL MODES =   6

    ANNULAR DUCT ANALYSIS USED

  J          GREC          GCYL          GANN

  1         .0000        7.5013        6.8531
  2       12.5664       11.7349       14.4285
  3       25.1327       15.2682       26.0950
  4       37.6991       18.6374       38.3452
  5       50.2655       21.9317       50.7513
  6       62.8319       25.1839       63.2209

 JR      HW ROOT          PROP CNST (RE,IM)    CUT-OFF FRQ    HW COR  AXL WVLNTH   MOD ANG
        ALPHA*R2                PER METER            HZ                    ft        deg

  1    6.853070     19.713180      .000000     612.231      2.21        .3187     26.97
```

```
 2    14.428500       4.913265       .000000    1288.996      1.05      1.2788     72.71
 3    26.095010      -2.491387     35.074630    2331.245       .58       .0000     90.00
 4    38.345170      -2.491387     58.102920    3425.634       .39       .0000     90.00
 5    50.751250      -2.491388     79.877620    4533.954       .30       .0000     90.00
 6    63.220940      -2.491389    101.210100    5647.956       .24       .0000     90.00

   PRESSURE AT SPL =      6.3246E+00 nt/m^2
   ENERGY IN J=1 MODE =      4.9441E-02 watts
   DESIRED MODE AMPLITUDE =      1.9178E+01 nt/m^2

INITIAL PISTON VELOCITY, INNER WALL =       .280375      .163253 m/sec
INITIAL PISTON VELOCITY, OUTER WALL =      1.000000      .000000 m/sec
INNER VELOC/OUTER VELOC =       .280375      .163253

 JR      EV-ALPHA                MODE C-VAL              MODE COEFF (RE,IM)      MAG MODE AMPL
        PER METER                                            nt/m^2                  nt/m^2

  1    11.241910      -.305718      .000000      1.917825E+01     1.324236E-08     1.9178E+01
  2    23.668810      -.960686      .000000     -9.313667E+00     2.115661E+01     2.3116E+01
  3    42.806770      1.222404      .000000      4.968037E-02     1.549457E-02     5.2041E-02
  4    62.902170       .355008      .000000      6.742401E-02     9.323716E-03     6.8066E-02
  5    83.253360       .063063      .000000      1.237546E-02     1.916386E-03     1.2523E-02
  6   103.708900      -.105775      .000000      2.008836E-02     2.430673E-03     2.0235E-02

   VELOCITY AT INNER WALL =     1.10319E-02  -1.78015E-02 m/s
   VELOCITY AT OUTER WALL =     1.77576E-03  -6.45257E-02 m/s
   DISPLACEMENT AMPLITUDE, INNER WALL =     9.72090E-05 in
   DISPLACEMENT AMPLITUDE, OUTER WALL =     2.99620E-04 in.
```

The output modes, normalized such that the first mode is unity, are given by

$A_1 = 1.0 + 0.0i$
$A_2 = -0.486 + 1.103i$

The second mode generated by the actuator rings does not closely match the desired fan source mode. A brief and cursory parametric study was made to attempt to find the inner wall actuator velocity that would match the desired mode coefficient, but this was unsuccessful in finding any improvement.

Since this is just a single example case, it offers neither proof nor ability to generalize, but it may indicate that there will be problems attempting to match two cut-on modes with coplanar actuator rings. Further investigation of the possible advantages of inner and outer rings is warranted, and is recommended for future effort.

4. Conclusions and Recommendations

4.1 Conclusions

An analysis has been developed to predict the modes generated in an annular duct due to the coupling of flush-mounted ring actuators on the inner and outer walls of the duct. The analysis has been combined with a previous analysis for the coupling of modes to a cylindrical duct in a FORTRAN computer program FDANC to perform the computations. The method includes the effects of uniform mean flow in the duct. The program can be used for design or evaluation purposes for active noise control hardware for turbofan engines.

Predictions for some sample cases modeled after the geometry of the NASA Lewis ANC Fan indicate very efficient coupling to the lowest order radial mode in both the inlet and exhaust ducts for the $m = 6$ spinning mode at frequencies where only a single radial mode is cut-on. Radial mode content in higher order cut-off modes at the source plane and the required actuator displacement amplitude to achieve 110 dB SPL levels in the desired mode were predicted. Equivalent cases with and without flow were examined for the cylindrical and annular geometry, and little difference was found for a duct flow Mach number of 0.1.

One case using both inner and outer actuator rings in a high-radius-ratio annular duct indicated that, when only one radial mode is cut-on, it might be possible to phase both rings to give a more efficient match to the desired mode than using only the outer ring. Whether the increased matching efficiency would justify the added hardware expense, however, is questionable.

One case was considered at a higher frequency in which two radial modes were cut-on, in a preliminary attempt to generate anti-phase matches to both modes using coplanar inner and outer actuator rings. In brief search, no combinations of inner and outer actuator velocity that matched the given modes could be found. Although the search was far from extensive, this may indicate that two coplanar rings may have a difficult time matching two arbitrary duct modes.

4.2 Recommendations for Further Effort

Further checkout and de-bugging of the prediction program is required to achieve a high level of confidence in its validity. This would include some parametric studies in which frequency, radius ratio, and flow Mach number are varied. It is recommended that the analysis be checked against test data obtained from ANC testing in the NASA Lewis 4-foot Fan Rig.

The actuator ring coupling program can be adapted as a subroutine to the cylindrical duct modal analysis and the exhaust duct modal analysis. This will allow the

fan source to be defined in terms of characteristic modes at the fan source plane and predict the propagation to the arbitrarily-located ANC source plane. The actuator velocities can then be determined to generate the anti-phase mode. The resulting combined fan source/ANC pressure can then be calculated at any desired wall sensor position. The actuator velocities can be determined manually or using a simulation of a control system feedback loop.

It would be useful to determine effects of higher Mach numbers on mode coupling, since this preliminary study went only to Mach 0.1 (representative of the flow in the NASA ANC fan). For the case with one radial mode cut-on, it would be useful to develop an optimization scheme that determines the inner wall actuator velocity that gives best coupling to the radial mode, and determine the implications of this increase in efficiency in terms of required power input, etc.

Finally, the possibility and limitations of coupling to two cut-on radial modes using coplanar inner and outer actuator rings should be examined. A plot of the mapping of the complex inner wall actuator velocity to the complex mode coefficient of the second radial mode could be made for specific cases. The implications of these results to design of feedback control systems should be explored.

5. Appendices

5.1 Appendix A - Numerical Computation of Bessel Function Integrals

The solution of the non-homogeneous differential equation that arises from the problem of the wall velocity boundary condition in the cylindrical duct requires the computation of four integrals involving Bessel functions of the first and second kind in the integrands. The integrals requiring evaluation are:

$$H_0^{mn} = \int_{r_1}^{r_2} \varphi_{mn}(\alpha_{mn} r) dr \tag{96}$$

$$H_1^{mn} = \int_{r_1}^{r_2} \varphi_{mn}(\alpha_{mn} r) r dr \tag{97}$$

$$H_2^{mn} = \int_{r_1}^{r_2} \varphi_{mn}(\alpha_{mn} r) r^2 dr \tag{98}$$

and

$$H_3^{mn} = \int_{r_1}^{r_2} \varphi_{mn}(\alpha_{mn} r) r^3 dr \tag{99}$$

where

$$\varphi_{mn}(\alpha_{mn} r) = J_m(\alpha_{mn} r) + C_{mn} Y_m(\alpha_{mn} r) \tag{100}$$

It may be possible to reduce the order of the Bessel function in the integration by using identities such as

$$\int x^n \varphi_{mn}(x) dx = -x^n \varphi_{m-1,n}(x) + (n + m - 1) \int x^{n-1} \varphi_{m-1,n}(x) dx \tag{101}$$

and, for certain m-values, this will reduce to a closed form in Bessel functions. Generally, however, one is left with the integral of a Bessel function that must be computed numerically, since there is no general integration formula for the integral

$$\int \varphi_{mn}(x) dx$$

where m is an arbitrary integer. Since one eventually ends up with an integral to be evaluated numerically, it seems more straightforward to simply integrate the original forms of the integrals by numerical integration.

A series of numerical integration subroutines have been adapted to evaluate these integrals. The subroutines are written in FORTRAN, suitable for use on the IBM-PC, and can be easily adapted to almost any other platform. The integrals are solved numerically by the Romberg integration method based on subroutines provided in *Numerical Recipes*[4]. The subroutine CBESEL, developed at GEAE, is used to compute the Bessel functions. The subroutines have been checked out against a MathCAD computation.

5.2 Appendix B - Contour Integrations for Inversion of Fourier Integrals

The Fourier Transform Inversion Integral required to find the z-dependent modal coefficients of the solution to the wall velocity boundary condition equation can be split into six separate integrals, which, in general form, are

$$G_j(z) = \frac{Q_{mn}^{(j)}}{2\pi} \int_{-\infty}^{\infty} \frac{\kappa^{j-1}\mathcal{H}(\kappa)e^{-i\kappa z}}{\left(k-\alpha_{mn}^2\right)+2kM\kappa-\left(1-M^2\right)\kappa^2}\,d\kappa \qquad (102)$$

for j = 1, 2, or 3, or

$$G_j(z) = \frac{Q_{mn}^{(j)}}{2\pi} \int_{-\infty}^{\infty} \frac{H_j(\kappa)e^{-i\kappa z}}{\left(k-\alpha_{mn}^2\right)+2kM\kappa-\left(1-M^2\right)\kappa^2}\,d\kappa \qquad (103)$$

for j = 4, 5, or 6, where the Q_{mn} are constant coefficients that depend on m and n. $\mathcal{H}(\kappa)$ is the Fourier Transform of the axial velocity function for the ANC noise source.

Following Butkov[5], these integrals can be evaluated as contour integrals in the complex plane using the theory of residues. The path of integration must be prescribed, taking into account poles in the complex plane. Assuming that the velocity function transforms $\mathcal{H}(\kappa)$ or $H(\kappa)$ have no zeros or poles in the region surrounded by the contour, the poles of the integrands of both integrals are at the complex points given by the roots of the denominator in the integrand:

$$\kappa^{\binom{1}{2}} = \frac{-kM \pm \sqrt{k^2-\left(1-M^2\right)\alpha_{mn}^2}}{1-M^2} \qquad (104)$$

Figure (13) shows the contour, which is chosen in a particular manner that results only in waves traveling in the positive z-direction. The contour consists of the negative and

positive real axis and a semi-circle of infinite radius that is closed downward. The integration direction is counter-clockwise. Since the semi-circular part of the integral at infinite radius doesn't contribute in the lower half plane $\{e^{i\kappa z} \to 0)$, the integral, by the residue theorem, is $2\pi i$ time the sum of the residues enclosed by the contour.

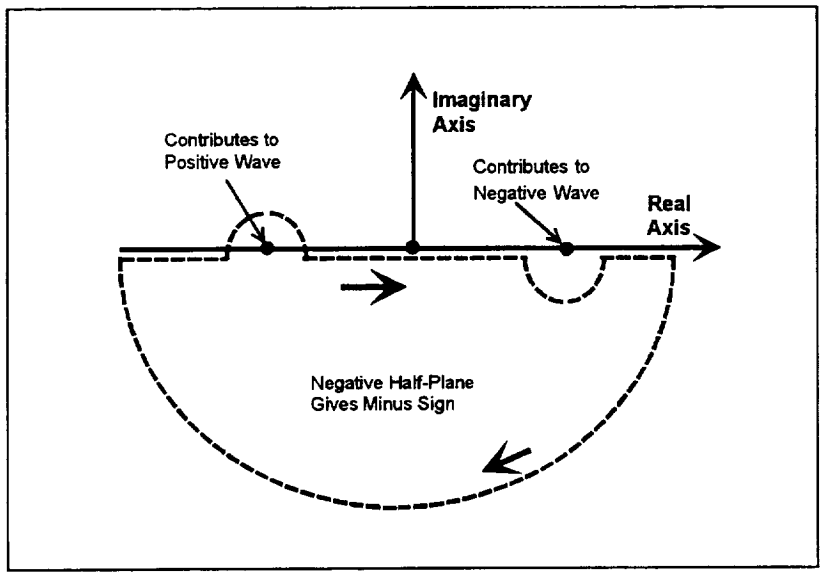

Figure (13) Shape of the contour for contour integration.

Thus

$$G_j(z) = -\frac{2\pi i Q_{mn}^{(j)}}{1-M^2}\,\mathrm{Res}\left[-\frac{1}{2\pi}\frac{\mathcal{H}(\kappa)\,e^{-i\kappa z}}{(\kappa-\kappa^{(1)})(\kappa-\kappa^{(2)})}\right]_{\kappa=\kappa^{(2)}} \tag{105}$$

and, since the residue at $\kappa = \kappa^{(2)}$ is

$$\lim_{\kappa\to\kappa^{(2)}}\left[-\frac{1}{2\pi}\frac{\mathcal{H}(\kappa)\,e^{-i\kappa z}}{\kappa-\kappa^{(1)}}\right] = -\frac{1}{2\pi}\frac{\mathcal{H}\left(\kappa^{(2)}\right)e^{+i\kappa^{(2)}z}}{\kappa^{(2)}-\kappa^{(1)}} \tag{106}$$

the first integral becomes

$$G_1(z) = -\frac{iQ_{mn}^{(1)}}{2}\frac{\mathcal{H}\left(-\kappa_{mn}^{+}\right)e^{i\kappa_{mn}^{+}z}}{\sqrt{k^2-\left(1-M^2\right)\alpha_{mn}^2}} \tag{107}$$

Following the same reasoning and using the same contour for the second integral, it becomes

$$G_j(z) = -2\pi i Q_{mn}^{(j)} \mathrm{Res}\left[-\frac{1}{2\pi} \frac{\kappa^{(j-1)} \mathcal{H}(\kappa) e^{-i\kappa z}}{(\kappa - \kappa^{(1)})(\kappa - \kappa^{(2)})} \right]_{\kappa = \kappa^{(2)}} \tag{108}$$

which, by the residue calculus, reduces to

$$G_j(z) = i\left(\kappa_{mn}^{+}\right)^{j-1} Q_{mn}^{(j)} \frac{\mathcal{H}\left(\kappa^{(2)}\right) e^{i\kappa^{(2)} z}}{\sqrt{k^2 - \left(1 - M^2\right)\alpha_{mn}^2}} \tag{109}$$

Making the correct substitutions for $\kappa^{(2)}$ and Q_{mn}, one can use these formulae to evaluate all required inverse transforms. The formulae apply to the cases with H_4, H_5, and H_6 if these transforms are sufficiently well-behaved, otherwise they must be evaluated as special cases.

6. References

[1] Kraft, R. E. and Kontos, K. B., "Theoretical Implications of Active Noise Control for Turbofan Engines", AIAA Paper 93-4355, October, 1993.

[2] Kraft, R. E., "Theory and Measurement of Acoustic Wave Propagation in Multi-Segmented Rectangular Flow Ducts", PhD Dissertation, University of Cincinnati, 1976, pp. 28-34.

[3] Kraft, R. E. and Kontos, K. B., "Theoretical Implications of Active Noise Control for Turbofan Engines", AIAA Paper 93-4355, October, 1993, pp. 5-7.

[4] Press, W. H., Flannery, B. P., Teukolsky, S. A., Vetterling, W. T., *Numerical Recipes: The Art of Scientific Computing*, FORTRAN Version, Cambridge University Press, 1986.

[5] Butkov, E., *Advanced Engineering Mathematics*, McGraw-Hill, 1966, p. 54547.

REPORT DOCUMENTATION PAGE

Form Approved
OMB No. 0704-0188

Public reporting burden for this collection of information is estimated to average 1 hour per response, including the time for reviewing instructions, searching existing data sources, gathering and maintaining the data needed, and completing and reviewing the collection of information. Send comments regarding this burden estimate or any other aspect of this collection of information, including suggestions for reducing this burden, to Washington Headquarters Services, Directorate for Information Operations and Reports, 1215 Jefferson Davis Highway, Suite 1204, Arlington, VA 22202-4302, and to the Office of Management and Budget, Paperwork Reduction Project (0704-0188), Washington, DC 20503.

1. AGENCY USE ONLY (*Leave blank*)	2. REPORT DATE	3. REPORT TYPE AND DATES COVERED
	September 1996	Final Contractor Report

4. TITLE AND SUBTITLE

Active Control of Fan Noise: Feasibility Study
Volume 6: Theoretical Analysis for Coupling of Active Noise Control Actuator Ring Sources to an Annular Duct with Flow

5. FUNDING NUMBERS

WU-538-03-11
C-NAS3-26617

6. AUTHOR(S)

R.E. Kraft

7. PERFORMING ORGANIZATION NAME(S) AND ADDRESS(ES)

General Electric Aircraft Engines
1 Neumann Way
P.O. Box 156301
Cincinnati, Ohio 45214-6301

8. PERFORMING ORGANIZATION REPORT NUMBER

E-10380

9. SPONSORING/MONITORING AGENCY NAME(S) AND ADDRESS(ES)

National Aeronautics and Space Administration
Lewis Research Center
Cleveland, Ohio 44135-3191

10. SPONSORING/MONITORING AGENCY REPORT NUMBER

NASA CR-198514

11. SUPPLEMENTARY NOTES

Project Manager, Laurence J. Heidelberg, Propulsion Systems Division, NASA Lewis Research Center, organization code 2770, (216) 433-3859.

12a. DISTRIBUTION/AVAILABILITY STATEMENT

Unclassified - Unlimited
Subject Categories 07 and 71

This publication is available from the NASA Center for AeroSpace Information, (301) 621-0390.

12b. DISTRIBUTION CODE

13. ABSTRACT (*Maximum 200 words*)

The objective of this effort is to develop an analytical model for the coupling of active noise control (ANC) piston-type actuators that are mounted flush to the inner and outer walls of an annular duct to the modes in the duct generated by the actuator motion. The analysis will be used to couple the ANC actuators to the modal analysis propagation computer program for the annular duct, to predict the effects of active suppression of fan-generated engine noise sources. This combined program will then be available to assist in the design or evaluation of ANC systems in fan engine annular exhaust ducts. An analysis has been developed to predict the modes generated in an annular duct due to the coupling of flush-mounted ring actuators on the inner and outer walls of the duct. The analysis has been combined with a previous analysis for the coupling of modes to a cylindrical duct in a FORTRAN computer program to perform the computations. The method includes the effects of uniform mean flow in the duct. The program can be used for design or evaluation purposes for active noise control hardware for turbofan engines. Predictions for some sample cases modeled after the geometry of the NASA Lewis ANC Fan indicate very efficient coupling in both the inlet and exhaust ducts for the m = 6 spinning mode at frequencies where only a single radial mode is cut-on. Radial mode content in higher order cut-off modes at the source plane and the required actuator displacement amplitude to achieve 110 dB SPL levels in the desired mode were predicted. Equivalent cases with and without flow were examined for the cylindrical and annular geometry, and little difference was found for a duct flow Mach number of 0.1. The actuator ring coupling program will be adapted as a subroutine to the cylindrical duct modal analysis and the exhaust duct modal analysis. This will allow the fan source to be defined in terms of characteristic modes at the fan source plane and predict the propagation to the arbitrarily-located ANC source plane. The actuator velocities can then be determined to generate the anti-phase mode. The resulting combined fan source/ANC pressure can then be calculated at any desired wall sensor position. The actuator velocities can be determined manually or using a simulation of a control system feedback loop. This will provide a very useful ANC system design and evaluation tool.

14. SUBJECT TERMS

Acoustic ducts; Active control; Fan noise; Ducted fans

15. NUMBER OF PAGES

43

16. PRICE CODE

A03

17. SECURITY CLASSIFICATION OF REPORT	18. SECURITY CLASSIFICATION OF THIS PAGE	19. SECURITY CLASSIFICATION OF ABSTRACT	20. LIMITATION OF ABSTRACT
Unclassified	Unclassified	Unclassified	